Morphology Evolution in Slowly Dip-Coated Supramolecular PS-b-P4VP Thin Films

ARTICLE *in* MACROMOLECULES · JULY 2012

Impact Factor: 5.8 · DOI: 10.1021/ma3007398

4 AUTHORS, INCLUDING:

Sébastien Roland
MINES ParisTech
8 PUBLICATIONS **51** CITATIONS

SEE PROFILE

Macromolecules

Article

pubs.acs.org/Macromolecules

Morphology Evolution in Slowly Dip-Coated Supramolecular PS-*b*-P4VP Thin Films

Sébastien Roland, David Gaspard, Robert E. Prud'homme,* and C. Geraldine Bazuin*

Département de chimie, Centre de recherche sur les matériaux auto−assemblés (CRMAA/CSACS), Université de Montréal, C.P. 6128 Succ. Centre−ville, Montréal (QC), Canada H3C 3J7

Supporting Information

ABSTRACT: Block copolymer films obtained by dip-coating have been much less studied than those obtained by spin-coating, although it is an important industrial process. In our investigations of supramolecular diblock copolymer films of PS−P4VP (~30 wt % P4VP) dip-coated from THF solutions, we initially found that films containing a monohydroxy-functionalized small molecule (SM), 1-naphthol (NOH), have a dot morphology, whereas those containing a monocarboxylic acid-functionalized small molecule, 1-naphthoic acid (NCOOH), have a stripe morphology. The COOH functionality is known to hydrogen bond more strongly to pyridine than OH. Yet the total amount of SM in the two types of films under given conditions is the same and PS−P4VP/NOH and PS−P4VP/NCOOH (equimolar SM:VP) in THF solution are both micellar, with the same spherical shape and size as PS−P4VP alone. On the other hand, the stripe morphology can be transformed to dot morphology by decreasing the dip-coating rate, the solution concentration or the SM:VP molar ratio, and vice versa. Vertical TEM indicates that the stripes correspond to horizontal cylinders, whereas the dots appear to be essentially spherical micelles. Although the films tend to be subject to terracing or dewetting, the average thickness of the films was observed to decrease toward a minimum with increase in dip-coating rate. This was related to the slow rates used, shown recently in sol−gel films to correspond to the so-called capillarity regime, and never before, to our knowledge, investigated in connection with its influence on block copolymer morphology. The minimum film thickness corresponds to the brush copolymer regime, which can be obtained almost uniformly for NOH-containing films, but is accompanied by stripe regions in the NCOOH-containing films investigated. Possible reasons for the differences in morphology evolution in films containing NOH vs NCOOH are discussed in the light of the experimental findings.

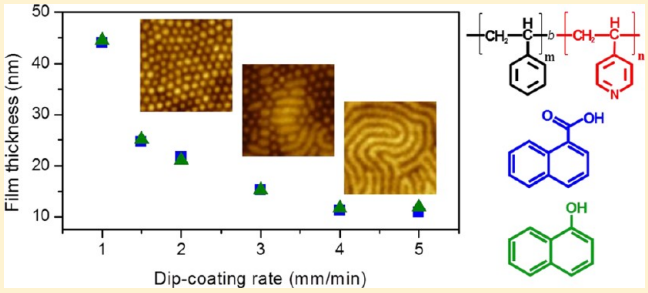

INTRODUCTION

The self-assembling properties of block copolymers in thin films have been investigated by numerous research groups for both their intrinsic scientific interest and their numerous potential nanotechnological applications, as summarized in a number of reviews (e.g., refs 1−7). The underlying phenomena of interest are the variety and orientation of the periodic structures to which the self-assembly gives rise, as dictated by various molecular and operational parameters. The latter are partially understood and are typically complicated by kinetic effects that can nevertheless be advantageous for obtaining desired patterns. It is known, for example, that factors controlling the film morphology and structural orientation include the block compositions, molecular weights and interaction parameters; interfacial interactions with substrate and air; film thickness relative to natural block copolymer periodicity; and type and evaporation rate of solvent used.

Among the many ways of controlling block copolymer thin film self-assembly, which is essential for applications, is the addition of block selective small organic molecules, particularly ones with functional groups that bond noncovalently to one of the blocks, also called "supramolecular control" or the "supramolecular approach".[8−15] [The addition of a homopolymer or second block copolymer, a related approach, may also be mentioned.[16−20]] One of the advantages of the use of small molecules is that they can be easily washed out to create porous materials useful for many applications.[5,8] They also provide a simple method for introducing other functionalities and/or hierarchical order into the films. More fundamentally, they participate in the different interactions, increase the mobility, and modify the relative phase fractions that are crucial for determining the final film morphology, and can thus be employed to control and to fine-tune the patterns. However, the phenomena involved are only beginning to be understood, and the supramolecular approach thus constitutes an emerging area in thin film research.[8d]

A block copolymer that is readily available in a large variety of block molecular weights and that is especially amenable to supramolecular control is polystyrene-*b*-poly(4-vinylpyridine) (PS−P4VP). Hence, it has been the most popular block

Received: April 10, 2012
Revised: June 11, 2012
Published: June 26, 2012

   dx.doi.org/10.1021/ma3007398 | Macromolecules 2012, 45, 5463−5476

copolymer with which functional small molecules have been associated, usually by hydrogen-bonding to the vinylpyridine (VP) group. In particular, ten Brinke and co-workers[13] and Tung et al.[9b−d] have associated 3-*n*-pentadecylphenol (PDP) with PS−P4VP, previously investigated in the bulk where structure-within-structure morphologies were found,[21] and were able to observe oriented hierarchical assemblies in thin films under certain conditions. Stamm and co-workers have used mainly 2-(4′-hydroxyphenylazo)benzoic acid (HABA), which possesses both a hydroxyl and a carboxylic acid H-bond donor, in conjunction with PS−P4VP.[8] They found that PS−P4VP/HABA films (typically with a P4VP/HABA volume fraction of ca. 0.25) dip-coated from dioxane solution lead to vertical cylinders whereas those prepared from chloroform solution lead to horizontal cylinders relative to the substrate. This cylinder orientation can be reversibly switched by annealing in the vapor of one or the other solvent. Furthermore, the film morphology can be manipulated by varying the HABA:VP molar ratio used.[8e] The film morphologies observed were interpreted in terms of how solvent swelling and selectivity move the system to different parts of the phase diagram.[8]

Of particular interest to the present study, mention was made that HABA-containing films dip-coated from THF solution give coexisting vertical and horizontal cylinders.[8a] In contrast, we found that films dip-coated from THF solutions of PS−P4VP with a ditopic molecule with two hydroxy groups, dihydroxynaphthalene (DHN), lead only to a dot (vertical cylinder or micelle) morphology whatever the relative DHN:VP ratio, the PS−P4VP composition, and film-forming conditions (in the ranges investigated).[10] Washing films with vertically oriented cylinders in methanol removes the small molecule, leaving nanoporous films.[8,10] These can be used as templates to grow, for example, metal nanodots.[8a,d,g]

Given the differing film morphologies obtained from THF solutions with HABA versus DHN, we decided to simplify the small molecule (SM) to a single functionality and compare the influence of a hydroxy-functionalized SM with an otherwise identical carboxylic acid-functionalized SM, thus decoupling the two types of hydrogen-bond functions. For this purpose, naphthol (NOH) and naphthoic acid (NCOOH) were chosen (Scheme 1). As briefly reported earlier,[10b] they lead to completely different morphologies, for which we use the terms dot and stripe morphologies, in dip-coated films. This is described in detail in the present paper, based on AFM studies, coupled with optical microscopy, cross-sectional TEM, and light scattering. We show how various compositional and experimental parameters, with particular focus on the dip-coating rate, influence the morphology obtained.

Scheme 1. Molecular Structure of the Two Principal Small Molecules Used in This Study

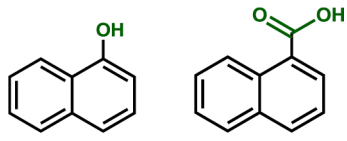

Furthermore, the vast majority of block copolymer thin films studied in the literature are obtained by spin-coating, where thickness can be controlled precisely by the solution concentration and spin-coating parameters. Only a few groups have looked closely at dip-coated films of block copolymers, although it is an important coating procedure industrially,[22] notably Stamm and colleagues[8] in the studies mentioned above, and Krausch and colleagues on films of PS-*b*-P2VP.[23] The present study therefore has additional interest in that it focuses on phenomena in dip-coated films, particularly in the so-called capillarity regime,[22] which is attained by the very slow dip-coating rates employed, and never before investigated, to our knowledge, in connection with block copolymer morphology.

EXPERIMENTAL SECTION

Materials. The polystyrene-*b*-poly(4-vinylpyridine) (PS−P4VP) block copolymers, whose molecular weight characteristics are given in Table 1, were purchased from Polymer Source (Dorval, QC) and used as received. They will frequently be referred to hereafter by their block molecular weights (in kg/mol), as in 71.9−30.2. The principal small molecules (SMs) employed were 1-naphthol (NOH, >99%, mp =95 °C; Sigma-Aldrich) and 1-naphthoic acid (NCOOH, 99.8%, mp =160−162 °C; Fluka), used as received. Other small molecules tested were 1-naphthalene acetic acid (97%, Sigma-Aldrich), 4′-hydroxy-4-biphenylcarboxylic acid (99%, Sigma-Aldrich), 3,5-dihydroxy-2-naphthoic acid (97%, Sigma-Aldrich), benzoic acid (99%, Mallinckrodt), *p*-toluic acid (98%, Sigma-Aldrich), 4-hydroxybenzoic acid (99%, Sigma-Aldrich), and 2,6-naphthalenedicarboxylic acid (99%, Sigma-Aldrich), all used as received. Tetrahydrofuran (THF, 99.99%; VWR) and methanol (MeOH, ≥99.9%; VWR) were used as received.

Table 1. Molecular Weight Characteristics of the PS−P4VP Block Copolymers Used[a]

M_n(PS)−M_n(P4VP) (kg/mol)	PDI	w_{P4VP} (%)	$w_{[P4VP+SM(1:1)]}$ NOH/NCOOH, (%)
71.9−30.2	1.13	29.6	50.0/52.6
31.9−13.2	1.08	29.3	49.6/52.2
78.9−30.3	1.22	27.7	47.6/50.3
41.5−17.5	1.07	29.7	50.0/52.7

[a] M_n: block molecular weight; PDI: polydispersity index; w_{P4VP}: weight percent of P4VP block in the block copolymer; $w_{[P4VP+SM(1:1)]}$: weight percent of the P4VP/SM phase, assuming equimolar incorporation of the SM in the P4VP phase (i.e., 1:1 VP:SM molar ratio; SM = NOH or NCOOH).

Solution Preparation. Unless otherwise specified, the block copolymer (BC) and small molecule, in a 1:1 SM:VP molar ratio, were dissolved together in THF to give a 0.5 wt % (5 mg/mL) solution concentration with respect to the BC. The solutions were stirred overnight at ca. 70 °C in sealed vials, and then filtered through a 0.45 followed by a 0.2 μm PTFE filter (Chromspec). The solutions were conserved in closed vials in the dark. No solutions older than one month were used, with reproducibility up to one month verified against fresh solutions.

Dip-Coating Procedure and Atomic Force Microscopy (AFM). Silicon wafers ({100}, 5 × 10 mm^2; University Wafer, Pittsburgh, PA) were used as substrates. These substrates (cleaned by soaking for several minutes in THF, wiping with Kimwipe tissue, and drying under nitrogen flow[24]) were dip-coated under ambient conditions (21 °C, variable humidity) by vertical immersion into solution at a rate of 5 mm/min, followed by a 30 s pause[24] and then vertical withdrawal from the solution at a controlled rate using a KSV 3000 Langmuir film balance. The coated substrates were air-dried in covered containers overnight. To remove the small molecule, the coated substrates were immersed in MeOH for 30 min, dried under nitrogen flow and then under vacuum at 70 °C for 5 min. AFM images were obtained in tapping mode with a Multimode microscope and a Nanoscope III controller (Digital Instruments) using the Nanoscope V5.30 software, operated under ambient atmosphere. The tips (Arrows

dx.doi.org/10.1021/ma3007398 | Macromolecules 2012, 45, 5463−5476

NC model; spring constant 42 N/m, oscillation frequency 285 kHz, tip radius <10 nm) were obtained from Nanoworld (Neuchâtel). Each experiment was repeated on at least two films, and often more, including from separate solution preparations. Film thicknesses were measured from large-scale (ca. 30 × 30 μm^2) AFM images across scalpel scratches. No significant differences in film morphology or thickness for any given dip-coating and composition condition were found in films dip-coated at different ambient humidities.

Fourier Transform Infrared Spectroscopy (FTIR). Transmission infrared spectra, obtained from an accumulation of 64 interferograms at a resolution of 4 cm^{-1}, were recorded with a Digilab Excalibur 3100 HE spectrometer equipped with a DTGS (deuterated triglycine sulfate) detector. Spectra were taken of films that were solution-cast on KBr pellets and dried overnight at 70 °C under vacuum and of the same films after immersion into anhydrous MeOH for 10 min, followed by drying at 70 °C under vacuum for 1 h. For the small molecules, ATR-IR spectra from an accumulation of 256 interferograms at a resolution of 4 cm^{-1} were taken on powder samples, using a hemispherical Ge ATR crystal and p-polarized radiation at a 65° incident angle and a Tensor Bruker spectrometer equipped with a MCT (mercury cadmium telluride) detector.

Solution Light Scattering. Dynamic light scattering measurements of 0.5 wt % THF solutions were made using a Brookhaven BI-200SM instrument equipped with a 532 nm laser. The measurements were made at an angle of 90° and a temperature of 20 °C, controlled by a thermostated circulating water bath. Each hydrodynamic radius was averaged over five measurements. Using the system software, the method of cumulants with the third-order model was applied to fit the normalized autocorrelation function.

Static light scattering measurements were made using a Wyatt Technology DAWN EOS multiangle spectrometer equipped with a 690 nm laser. The solutions were manually injected using a HPLC pump with a 2-mL injection loop at a rate of 0.3 mL/min. Zimm plots were obtained using the ASTRA V.5.3.4.20 software for six different concentrations of copolymer solutions in THF (ranging from 0.05 to 0.3 mg/mL). The radii of gyration were calculated from the Zimm plots.

Optical Microscopy. Optical micrographs were obtained using a Zeiss Axioskop 40 optical microscope with nonpolarized incident light in reflection mode.

Transmission Electron Microscopy (TEM). In-plane TEM images were taken with a JEOL JEM 2000FX instrument operated at 80 kV. Prior to film deposition, freshly cleaved mica substrates were carbon coated (using a Cressington 108 carbon/A vacuum carbon evaporator) to facilitate film detachment. Film deposition followed the same procedure as for AFM. The films were detached from the substrate by floating in water. They were then transferred onto copper grids, dried and exposed for 24 h to I_2 vapor, which selectively stains P4VP.

Cross-sectional (out-of-plane) TEM images were taken with a Philips Tecnai 12 operated at an acceleration voltage of 80 kV. Prior to dip-coating, the silicon substrates used were thermally annealed overnight in an oven at 700 °C in ambient atmosphere to create a thicker oxide layer, which eases the floating of the films on a 5 wt % hydrofluoric acid (HF) solution due to dissolution of the silicon oxide layer by the acidic solution.[16d] The floating films were picked up with pieces of cured epoxy (Embed-812, Electron Microscopy Sciences), allowed to dry, then covered with fresh epoxy and cured at 40 °C for 48 h. The cured epoxy-embedded films were then microtomed perpendicular to the film plane into slices of approximately 70–80 nm thick, using a Reichert-Jung Ultracut E microtome equipped with a Drukker diamond knife. Finally, the slices were deposited on Formvar–carbon coated copper TEM grids (Mecalab) and exposed for 3 h to I_2 vapor.

RESULTS AND DISCUSSION

Infrared Evidence for H-Bonding. Since THF is a competitive H-bond acceptor[9e] and could thus, at least partially, freeze out SM-VP H-bonding in the dried films, the state of NOH and NCOOH H-bonding with the PS–P4VP block copolymer (BC), 71.9–30.2, in solvent-cast films should be verified. The OH–pyridine hydrogen bond is considered to be intermediate in strength, whereas the COOH–pyridine hydrogen bond is considered to be strong.[25] Figures 1 and 2 show the IR spectra of THF solution-cast films of the two PS–P4VP/SM (SM:VP 1:1) systems before and after rinsing with methanol compared with those of the respective components. H-bonding in the BC/NOH system (Figure 1) is shown by the shift of the free pyridine bands at 993 and 1415 cm^{-1} for the copolymer to about 1007 (as a shoulder on a NOH band) and 1420 cm^{-1}, respectively, for the blend.[10,21b,26] In addition, the composite aromatic band at 1598 cm^{-1} (free pyridine in P4VP, phenyl in PS, aromatic rings in NOH) shows the presence of an additional peak for the blend at ca. 1603 cm^{-1} attributed to H-bonded pyridine.[26,27] H-bonding in the BC/NCOOH blend (Figure 2) is shown by the shift of the same pyridine bands to 1013, 1417 and a clearly distinguished peak at 1605 cm^{-1}, respectively,[25,28] with additional evidence provided by the two broad bands at ca. 2500 and 1950 cm^{-1}, which are a signature of strong carboxylic acid–pyridine hydrogen bonds.[25,28,29] Furthermore, the carbonyl band at 1676 cm^{-1} for NCOOH,

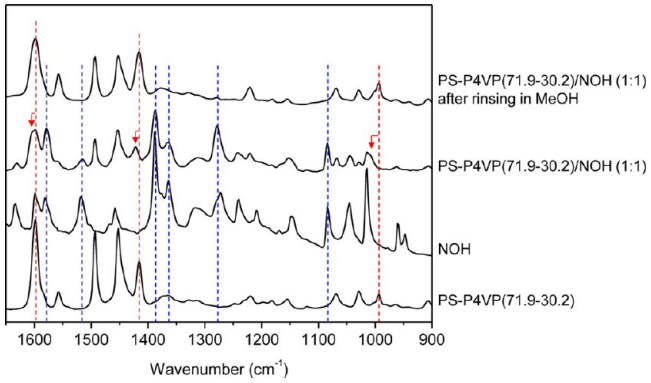

Figure 1. Infrared spectra of a PS–P4VP (71.9–30.2) film, naphthol (NOH), and a PS–P4VP/NOH (1:1) film before and after rinsing in methanol. The red dashed lines highlight VP bands that are shifted, as indicated by the arrows, in the BC/NOH blend (see text). The blue dashed lines highlight selected NOH bands.

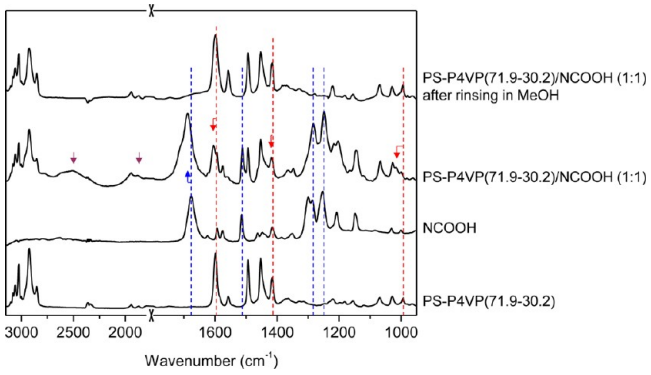

Figure 2. Infrared spectra of a PS–P4VP (71.9–30.2) film, naphthoic acid (NCOOH), and a PS–P4VP/NCOOH (1:1) film before and after rinsing in methanol. The red dashed lines highlight VP bands that are shifted, as indicated by the arrows, in the BC/NCOOH blend (see text). The blue dashed lines highlight selected NCOOH bands, the arrow indicating the shift in the carbonyl band. Prune arrows indicate new bands indicative of strong COOH–VP H-bonds.

dx.doi.org/10.1021/ma3007398 | Macromolecules 2012, 45, 5463–5476

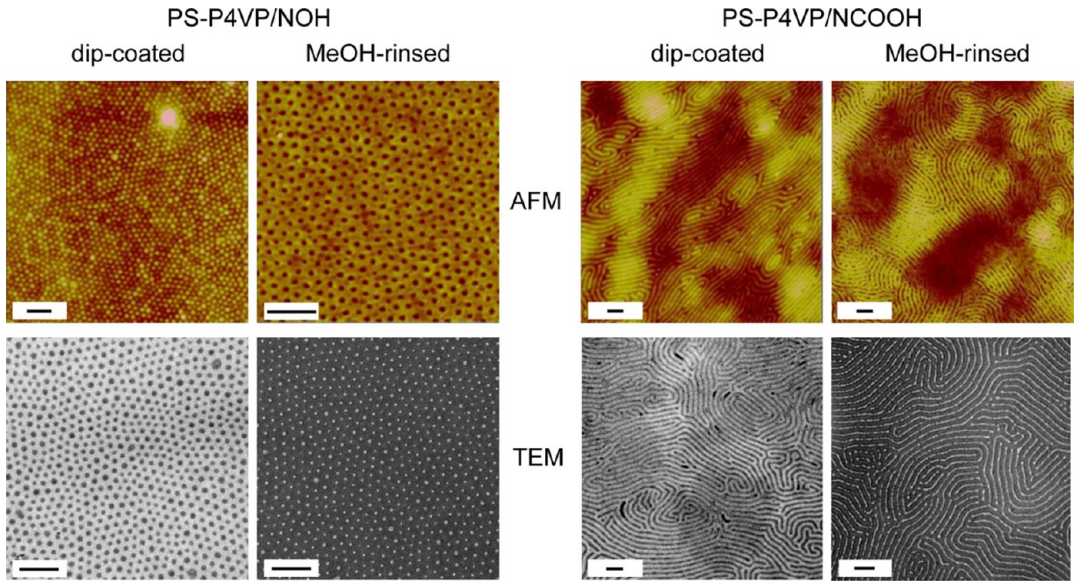

Figure 3. AFM height images and TEM micrographs of thin films of PS−P4VP(71.9−30.2)/SM blends (1:1 SM:VP; SM = NOH, NCOOH) dip-coated from THF solution at a rate of 2 mm/min, before and after rinsing in MeOH. The scale bars represent 200 nm. The z-ranges for the AFM images are, from left to right, 0−12, 0−20, 0−11, and 0−20 nm, respectively.

attributed to hydrogen-bonded acid dimers, is shifted to 1695 cm^{-1} in the BC/NCOOH blend, indicating that the OH group of the acid is H-bonded to VP, freeing the C═O group from H-bonding.[25,28]

The quasi-disappearance of the 993 cm^{-1} free pyridine band in both blends indicates that the extent of SM/VP hydrogen bonding in these equimolar blends is close to complete, although the weak shoulder on the high wavenumber side of the carbonyl band, which is ascribed to free acid groups, indicates the presence of a small fraction of free NCOOH molecules. The spectra of the films after rinsing in MeOH show that the small molecules are essentially completely washed out in both cases, as evidenced by the return of the above-mentioned pyridine bands to their original positions and by the disappearance of the various NOH bands (e.g., those at 1388 and 1516 cm^{-1}) and NCOOH bands (e.g., the carbonyl bands and that at 1510 cm^{-1}) as well as, in the latter case, of the broad bands at 2500 and 1950 cm^{-1}.

Dip-coated thin films similarly show clear evidence by IR of H-bonding between the SMs and the P4VP block.[30] Very importantly, as will be described in detail in a forthcoming paper, it was found that the amount of SM in the dip-coated film is less than in solution and increases with dip-coating rate, but is the same within experimental uncertainty for both NOH and NCOOH for a given condition (dip-coating rate, solution SM:VP ratio).[30] As points of reference, the relative proportion of the P4VP phase increases from almost 30 wt % for pure PS−P4VP to a maximum of ca. 50 wt % assuming equimolar SM:VP in the P4VP phase (Table 1). In the bulk, 30 wt % (≈ 30 vol %) P4VP is very near the transition from cylindrical to lamellar equilibrium morphology,[21b] so that even moderate swelling of P4VP by the SM puts the bulk system in the composition range for lamellar morphology.

Effect of NOH vs NCOOH on Thin Film Morphology. Representative AFM height images and TEM micrographs of thin films that were dip-coated under identical conditions at a withdrawal rate of 2 mm/min onto silicon substrates from 0.5 wt % THF solutions of PS−P4VP/SM (1:1 SM:VP; SM = NOH and NCOOH), followed by removal of the SM by rinsing in MeOH, are given in Figure 3. They show that the NOH-containing film has a very different morphology from the NCOOH-containing film, despite the fact noted above that the total amount of SM in the films is the same for both NOH and NCOOH under the same experimental conditions and despite the fact that their film thicknesses, to be discussed below, are similar (20−25 nm). NOH leads to the same quasi-hexagonal pattern of P4VP/SM nodules within a PS matrix as observed previously with DHN,[10] whereas NCOOH gives a fingerprint pattern of regularly alternating PS and P4VP/SM stripes. This is indicated for the NOH blend by the light-colored (protruding) dots within a darker (lower-lying) matrix in the AFM height image and by the dark (I_2-stained P4VP) dots in a light-colored (unstained PS) matrix in the TEM image. The protrusion of the P4VP/NOH nodules by about 3 nm above the PS matrix can be ascribed to the greater shrinking of the initially THF-swelled PS compared to the much less swelled P4VP phase.[10,31] For the NCOOH system, the lighter-colored (higher) stripes or ridges that alternate with darker-colored (lower) stripes or grooves (height difference ∼2 nm) in the AFM images reflect the alternation of the P4VP/NCOOH and PS phases, respectively. In TEM, these are observed as dark (I_2-stained), narrow P4VP/NCOOH stripes interspersed by light-colored (unstained) PS stripes. As will be shown below by cross-sectional TEM, the dots appear to be spherical micelles and the stripes in-plane cylinders.

For both SM-containing films, the general patterns obtained in the dip-coated films are maintained after the MeOH wash due to anchoring by the vitreous PS matrix, except that, in the NOH film, the nodules are replaced by smaller-diameter pores (dark in the AFM image, light in the TEM image) and, in the NCOOH film, the originally higher P4VP/NCOOH stripes are transformed into narrow and somewhat discontinuous grooves (dark and light in the AFM and TEM images, respectively), leaving the PS phase as ridges. These pores and grooves (which are 13 ± 2 and ∼10 nm in depth, respectively, and which therefore do not fully penetrate the films in accordance with the spherical and in-plane cylindrical morphologies) are a result, in part, of the washing out of the small molecule (as shown above

dx.doi.org/10.1021/ma3007398 | Macromolecules 2012, 45, 5463−5476

Table 2. Hydrodynamic Radii (R_h) and Radii of Gyration (R_g) of Two PS−P4VP Block Copolymers in THF, with and without Equimolar SM (NOH or NCOOH; SM:VP 1:1)

	78.9−30.3			41.5−17.5		
	SM-free	NOH	NCOOH	SM-free	NOH	NCOOH
R_h (nm)	34.5 ± 0.3	34.8 ± 1.1	34.5 ± 0.5	27.1 ± 0.4	26.4 ± 0.4	26.2 ± 0.1
R_g (nm)	25.4 ± 0.9	ND[a]	25.5 ± 1.0	19.2 ± 4.8	19.1 ± 4.2	19.6 ± 2.8
R_g/R_h	0.736	ND	0.735	0.708	0.723	0.748

[a]ND: not determined.

Table 3. Film Morphologies (Morph) and Lateral Periodicities (Period) of Dip-Coated Films of PS−P4VP/SM (SM = NCOOH, NOH) Obtained from 0.5 wt % THF Solutions (1:1 SM:VP) at the Dip-Coating Rates Indicated[a]

		41.5−17.5					78.9−30.3			
	31.9−13.2 NCOOH	NCOOH		NOH		71.9−30.2 NCOOH	NCOOH		NOH	
dip-coating rate (mm/min)	morph	morph	period (nm)	morph	period (nm)	morph	morph	period (nm)	morph	period (nm)
0.1	d									
0.5	d					d				
1	d/s	d	57L/53H	d	52L/48H	d	d	66L/60H	d	50
1.5		d/s	64/59	d	49	d/s	d	67		
2	s	s	57	d	51	s	d	71	d	56
3	s	s	55	d	52	s	d	74	d	61
4	s	s	54	*b*		s	d/s	74/71	d	66
4.5							s(+d)	67s		
5	s	s	56	*b*		s	s(+d)	66s	d	70
6							s		d	71
7							s		d	74
8							s		d	75

[a]Key: d = dots; s = stripes; L, lower terrace (T1), H, higher terrace (T2); always T1 for 1.5 mm/min and higher. [b]Featureless (see text for details).

by infrared spectroscopy) from a film whose integrity is preserved by the glassy PS matrix (insoluble in MeOH), leaving behind a shrunken P4VP phase and therefore P4VP-lined holes (pores and grooves). The gray-colored matrix in the TEM images of the films after rinsing is attributed to part of the P4VP having been washed up onto the film surface, as shown by Tokarev et al.[8b] for the HABA system using X-ray photoemission spectroscopy and by Laforgue et al.[10a] for the DHN system using water contact angle measurements. This partial relocation of P4VP to the surface, also termed surface reconstruction,[32] contributes to the formation of the pores and grooves. In addition, there is an ultrathin interfacial layer (also called "wetting" and sometimes "adaptive"[8] layer) next to the substrate, as deduced by Tokarev et al.[8b] for the HABA system based on X-ray reflectometry data and by Laforgue et al.[10] for the DHN system based on cyclic voltammetry data. The morphology observed is indifferent to the type of substrate used (here, silicon for AFM and carbon-coated mica for in-plane TEM), as also found previously and attributed to the adaptive behavior of the wetting layer.[8,10a]

Several other small molecules with OH and/or COOH groups were tested under the same dip-coating and solution conditions as above, but using the 41.5−17.5 copolymer. The three COOH-monofunctionalized SMs tested, benzoic acid, p-toluic acid and 1-naphthalene acetic acid, give the stripe morphology like NCOOH. It may be mentioned that Kuila et al. found that the COOH-monofunctionalized molecule, 1-pyrenebutyric acid, also provokes a stripe morphology (considered to be side-on lamellae in this case) for a PS−P4VP (32.9−8.0) dip-coated from dioxane solution (1:1 SM:VP).[33] On the other hand, ditopic 4-hydroxybenzoic acid and 4′-hydroxy-4-biphenylcarboxylic acid, each with an OH and a COOH group at opposite ends of the molecule, as well as 3,5-dihydroxy-2-naphthoic acid, possessing one COOH and two OH groups, give the dot morphology (IR spectra given in Figure SI-1 in the Supporting Information). Investigation involving these molecules was not pursued, to focus on NOH and NCOOH.

Solution Characterization by Light Scattering. It is known that PS−P4VP BCs give micellar solutions in many solvents, including THF.[34] To determine if the small molecule (NOH or NCOOH) modifies the micelle characteristics to thereby influence the film morphology, the hydrodynamic radii (R_h) and radii of gyration (R_g) were determined by dynamic and static light scattering (DLS and SLS), respectively, for the BCs, 78.9−30.3 and 41.5−17.5, in THF without and with SM present (1:1 SM:VP) (Table 2). Both techniques confirm that the solutions are micellar and show that the micellar size is identical within experimental uncertainty for a given copolymer whether or not the SM is present. The R_g/R_h ratio, from which the shape of the micelles can be inferred, indicate that they are spherical ($R_g/R_h \leq 0.775$)[34] in all cases. The significantly lower values of this ratio compared to that for hard spheres (0.775)[34] indicates "soft" spherical micelles,[35] which can be related to THF swelling. The fact that the addition of NOH or NCOOH to the solution influences neither the size nor shape of the micelles is consistent with THF being a competitive H-bond acceptor, and it can be concluded that the solution characteristics cannot account for the different morphologies in NOH and NCOOH-containing films.

Effect of Dip-Coating Rate. The initial investigations of the NOH- and NCOOH-containing systems were conducted

dx.doi.org/10.1021/ma3007398 | Macromolecules 2012, 45, 5463−5476

using the 71.9−30.2 copolymer, which, when no longer available, was replaced by a copolymer with very similar molecular weight characteristics, namely 78.9−30.3. This initially led to a surprise, in that the NCOOH-containing 78.9−30.3 film dip-coated under exactly the same conditions as the NCOOH-containing 71.9−30.2 film led to the dot rather than the stripe morphology. It was then discovered that another important parameter affecting the morphology is the dip-coating rate, verified for four different copolymers (Table 1), all of very similar block fractions; namely, the two just mentioned and two others of approximately half the total molecular weight (31.9−13.2 and 41.5−17.5). The morphologies observed at different dip-coating rates for these polymers are summarized in Table 3, with selected AFM images for 71.9−30.2/NCOOH films shown in Figure 4. The data in Table 3 indicate that, when

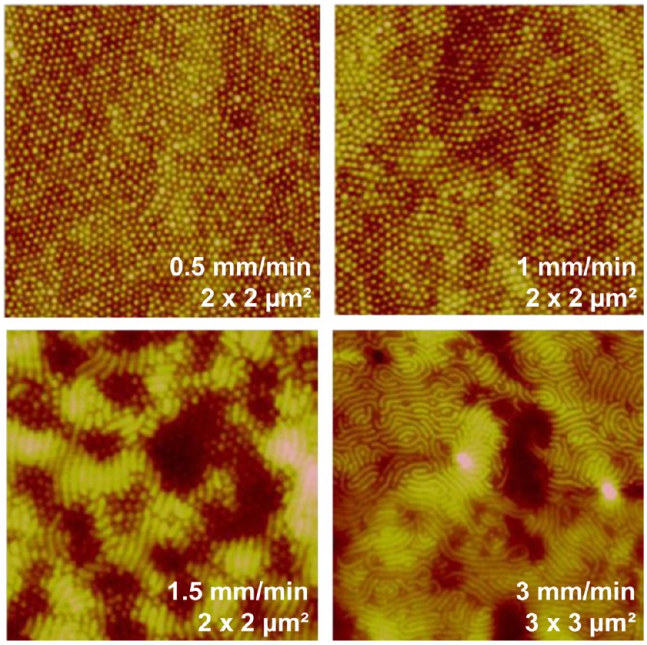

Figure 4. AFM height images of thin films of PS−P4VP(71.9−30.2)/NCOOH (1:1 NCOOH:VP) dip-coated from THF solution at the dip-coating rates indicated.

the stripe morphology is obtained, sufficient reduction of the dip-coating rate will yield the dot morphology. In contrast, no stripe morphology was found for the NOH system, investigated over a comparable range of dip-coating rates with the two copolymers, 78.9−30.3 and 41.5−17.5 (but see below for the effect of solution concentration). It must be added that, at the highest dip-coating rates used, the stripe morphology in NCOOH-containing films is accompanied by regions of featureless morphology and NOH-containing films become entirely featureless (see below).

The dip-coating rate at which the dot−stripe transition for the NCOOH-containing systems occurs is approximately the same for three of the four BCs investigated, namely about 1.5 mm/min (this rate was not investigated for 31.9−13.2, but, in this case, a mixture of stripes and dots are observed for 1.0 mm/min). Only the 78.9−30.3 BC reproducibly shows the transition at a much higher dip-coating rate (4−5 mm/min). Given the similarity of the total molecular weight and relative block content of all four BCs, it does not seem plausible to attribute the different transition rate for 78.9−30.3 to either of these parameters (besides, a 32.9−8.0 BC with 19.6 wt % VP content also showed a transition rate of 1.5 mm/min); perhaps it is related instead to its higher polydispersity or some other undetected particularity of this polymer.

Effect of SM:VP Molar Ratio. The film morphology was found to be influenced by the SM:VP molar ratio in solution for NCOOH-containing films, but not for NOH-containing films in the range and conditions investigated. For the 78.9−30.3 copolymer, an increase in the solution NCOOH:VP molar ratio from 1:1 to 2:1 at a dip-coating rate of 2 mm/min changes the morphology from dot to stripe (at a molar ratio of 3:1, the morphology appears poorly defined), as opposed to only the dot morphology for the NOH system for the 1:1 to 3:1 molar ratios. Furthermore, when the dip-coating rate for the 2:1 molar ratio NCOOH system is reduced to 1 mm/min, the stripe morphology reverts back to the dot morphology, consistent with the observation above concerning the influence of dip-coating rate on the stripe morphology. The effect of the solution NCOOH:VP molar ratio will be analyzed in detail elsewhere, in conjunction with the infrared determination of this ratio in dip-coated films.[30]

Effect of Solution Concentration. As shown in Table 4, another parameter that influences the film morphology is the

Table 4. Film Morphology of PS−P4VP/SM Block Copolymers Dip-Coated from THF Solutions (SM:VP 1:1) of Various Concentrations and Dip-Coating Rates (mm/min)[a]

	PS-P4VP concentration (wt %)							
	70.9−30.2			78.9−30.3			41.5−17.5	
SM (rate)	(0.25)	(0.5)	(1.0)	(0.25)	(0.5)	(1.0)	(0.5)	(1.0)
NOH (2)		d			d		d	d
NOH (5)					d		d	s
NCOOH (2)	d	s	s	d	d	d	s	
NCOOH (3)		s		d	d	s	s	

[a]Key: d = dot; s = stripe.

solution concentration, which yields thicker films for a given dip-coating rate.[22] First, it was found that lowering the concentration of the 70.9−30.2/NCOOH system in THF to 0.25 wt %, using the usual dip-coating rate of 2 mm/min, changes the stripe morphology to dot, while the morphology remains in the form of stripes for 1.0 wt % concentration. Conversely, for the 78.9−30.2/NCOOH system, the dot morphology is still obtained for a solution concentration of 1.0 wt % using the dip-coating rate of 2 mm/min; however, at 3 mm/min, this concentration produces the stripe morphology. In other words, higher solution concentrations favor the stripe morphology. With this in mind, an NOH system was also investigated at a higher solution concentration, notably 1 wt % with the 41.5−17.5 BC, and it was finally discovered that the stripe morphology is also possible with NOH (Table 4). Specifically, whereas the dot morphology was produced from this concentration using dip-coating rates of up to 4 mm/min, the stripe morphology was obtained using 5 mm/min. Furthermore, the 31.9−13.2/NOH system produces the stripe morphology for both 0.5 and 1 wt % concentrations using the 2 mm/min dip-coating rate.

A dependence of morphology on the concentration of the dip-coating solution was previously observed by Krausch and colleagues for PS−P2VP films dip-coated from a micellar

dx.doi.org/10.1021/ma3007398 | Macromolecules 2012, 45, 5463−5476

toluene solution.[23] They found that an increase in concentration transforms the morphology from large isolated circular micelles (dots) to smaller, hexagonally packed dots, and then to stripes (wormlike micelles, ribbons). At still higher concentration, the morphology reverts back to (disordered) dots, correlated with the development of a second layer of circular micelles on top of the first layer (resulting in a nonflat film surface). The transition from circular to wormlike micellar morphology as a function of solution concentration was observed for both symmetric and asymmetric BCs.[23a]

Film Thickness. It is known that, in general, the rate of dip-coating from polymer solutions influences the polymer film thickness,[22,36] and for block copolymers, the film thickness influences the film morphology.[1] As will be shown in the next section, the films investigated here are generally not uniform in thickness, although this does not affect the morphology observed in a given film. Nevertheless, an average thickness can be estimated, as determined from large-scale AFM images (typically 30 × 30 μm), that gives an idea of the relative amount of material deposited on the substrate. These values are plotted in Figure 5 for the various systems studied.[37] In all cases,

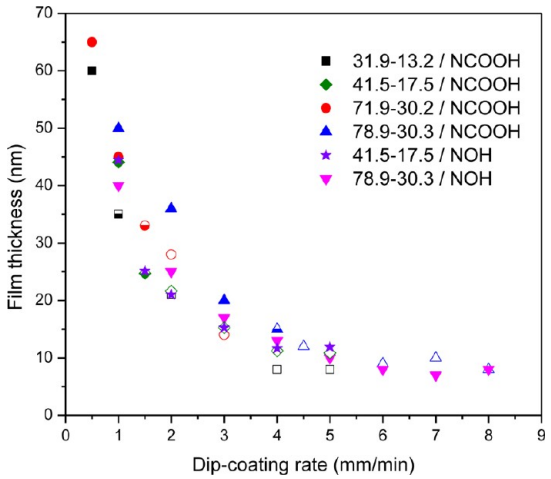

Figure 5. Average film thickness as a function of dip-coating rate for films obtained from THF solutions of 0.5 wt % of various PS−P4VP block copolymers with SM (NOH or NCOOH; SM:VP 1:1). The morphologies of the films are indicated by closed symbols for dots, open symbols for stripes, and half-closed symbols for mixed dots and stripes.

including for both the NOH and the NCOOH systems, the average thickness for a given dip-coating rate is similar, and it decreases with increasing dip-coating rate, tending toward a constant in the higher range of dip-coating rates used. It is noteworthy that, although the stripe morphology is observed only in the thinner films, there appears to be no particular critical film thickness where the dot-stripe transition occurs (the filled and open symbols in Figure 5 representing the two morphologies, respectively); that is, some films displaying the dot morphology are thinner than others displaying the stripe morphology and vice versa. This means that film thickness by itself does not govern the film morphology obtained. It also suggests that there is no significant difference in viscosity between NOH- and NCOOH-containing solutions, since viscosity differences should result in different film thicknesses.

The decrease in film thickness with increasing dip-coating rate is contrary to what is usually observed for dip-coated films.[22,36] However, Grosso and colleagues,[22] who investigated sol−gel films dip-coated over a wide range of dip-coating rates, showed that the film thickness does indeed decrease with dip-coating rate for very low rates, reaches a minimum, and then rises with dip-coating rate. The first regime, which they term the "capillarity regime", is governed by capillary rise and solvent evaporation, and has only rarely been investigated up to now. The regime following the minimum, termed the "draining regime", covers the dip-coating rates most often used; it is governed by gravity-induced viscous drag, first modeled long ago by Landau and Levich for Newtonian fluids.[22,38] Assuming the general applicability of this V-shaped dependence, the films of the present study have clearly been dip-coated in the capillarity regime, attaining the minimum thickness at the highest rates used. This minimum thickness is obtained at dip-coating rates (ca. 6−8 mm/min) that are in the range observed for the minimum in the sol−gel films investigated by Grosso and colleagues (between 0.1 and 1 mm/s).[22] In our NOH-containing films, this thickness, as will be shown below, corresponds essentially to an adsorbed monolayer or the brush regime of the BC where no in-plane phase-separated morphology is observed.

In contrast to our dip-coating conditions, the PS−P2VP films of Krausch and colleagues mentioned above were dip-coated on the opposite side of the minimum; that is, in the draining regime (mm/s compared to our mm/min).[23d] Their observation that the film thickness increases with dip-coating rate is consistent with this. Furthermore, they describe a regime, reached by decreasing the dip-coating rate sufficiently, where no micelles (dots) are formed.[23d] The rates involved, which depend on the solution concentration, are comparable to those giving the brush regime in our films. Evidently, the same minimum thickness giving the brush monolayer film has been reached in both ours and the Krausch systems, but arriving from opposite sides of the minimum in the V-shaped curve. The combined observations for ours and the Krausch systems also support the generality of the relationship described by Grosso and colleagues. The films studied by Stamm and colleagues were likewise dip-coated in the draining regime extending from the minimum (0.1−1.0 mm/s), although, to our knowledge, the effect of dip-coating rate was not specifically investigated.[8] In the light of these insights, investigations at higher dip-coating rates are underway in our laboratory to compare how the morphologies evolve from the capillarity regime across the minimum into the draining regime.

Terracing/Dewetting Phenomena. The dip-coated films of the present study are, in reality, subject to a form of terracing, examined in detail using the 41.5−17.5 BC. The thickness variations are illustrated by the representative optical microscopy (OM) images in Figure 6, where the lighter the color, the thinner the film. For a dip-coating rate of 1 mm/min, three levels of thickness can be clearly distinguished for both the NOH and NCOOH systems: the thinnest parts are found in the central portion of relatively large blobs or cells (between which are smaller blobs), and a thicker region in the outer portions. The blobs are outlined by still thicker areas in the form of ridges, sometimes only partially (see Figure 7 for the NCOOH system), which may be related to ambient temperature differences during dip-coating that modify film thickness in the capillarity regime.[22] AFM topographic images of the various regions show that all of them are characterized by the nodular morphology for both NCOOH-containing (Figure 7) and NOH-containing (Figure SI-2, Supporting Information)

dx.doi.org/10.1021/ma3007398 | Macromolecules 2012, 45, 5463−5476

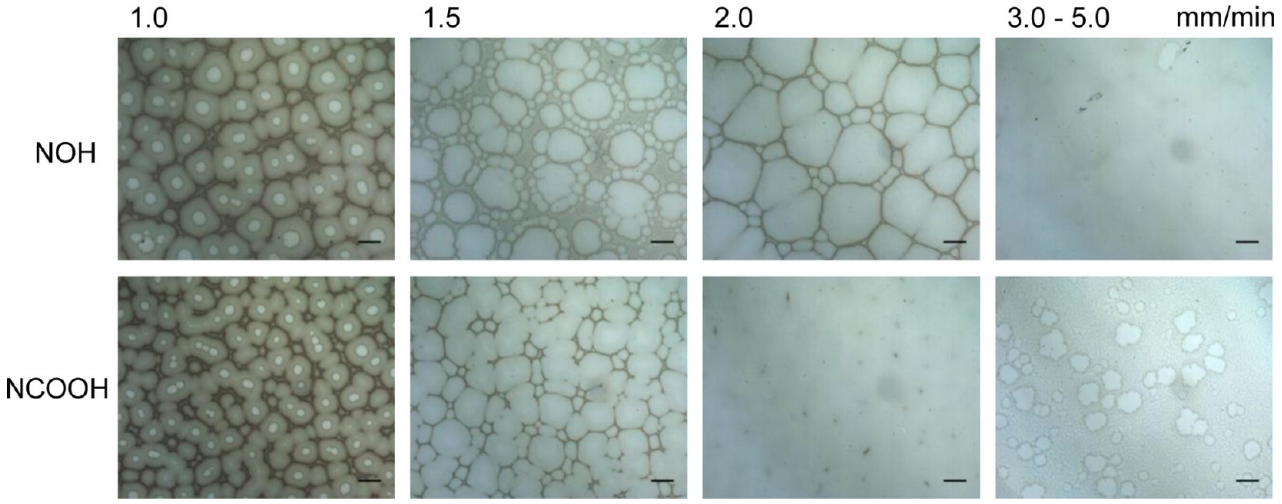

Figure 6. Optical micrographs of thin films of equimolar PS−P4VP(41.5−17.5)/SM (SM = NOH, NCOOH) at the dip-coating rates indicated. Scale bars: 25 μm.

films. From scratches on large-scale AFM images allowing the thicknesses of the different regions to be determined, and in conjunction with cross-sectional TEM images (see below), they might be identified (in order of increasing thickness) as monolayers and bilayers of spheres, with the ridges corresponding to a much smaller fraction of trilayers. Although these layers are less well-defined in thickness compared to terraces in solvent-annealed films, we will refer to them for convenience as T1, T2, and T3, respectively. The T1 regions are topographically relatively smooth on the micrometer scale, whereas the T2 regions tend to show greater roughness, especially for the NCOOH system as shown in Figure 7 (see Figure SI-2, Supporting Information, for the NOH system).

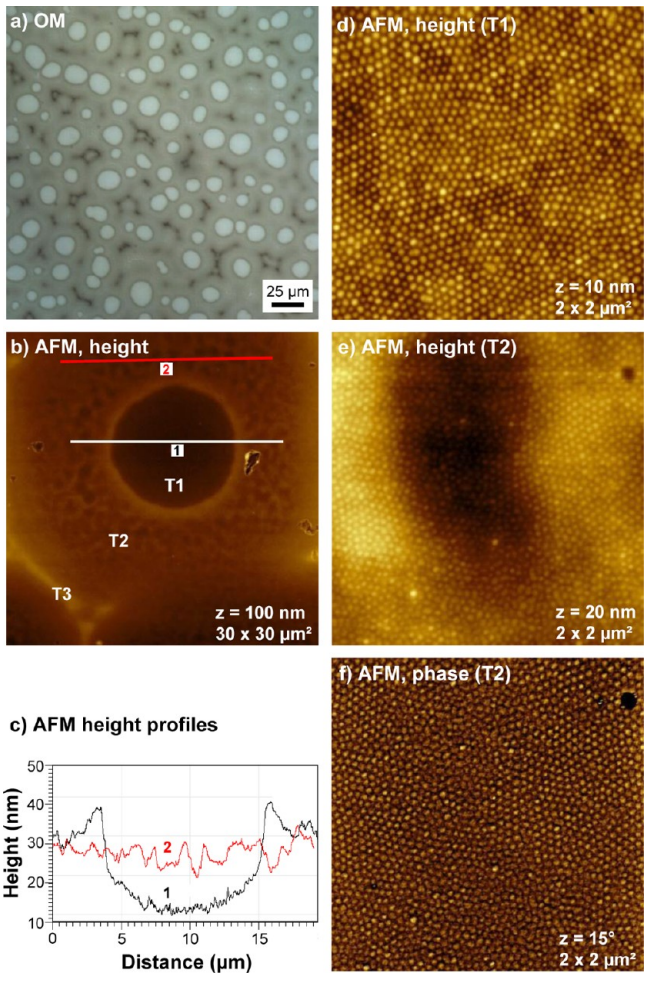

Figure 7. Optical microscopy (a) and AFM images (b, d−f) of an equimolar PS−P4VP(41.5−17.5)/NCOOH film dip-coated at a rate of 1 mm/min. Images e (height) and f (phase) are of the same spot. The height profiles in part c follow the lines indicated in part b.

Increasing the dip-coating rate to 1.5 mm/min reduces the observed thickness levels observed in OM to two, with T1 dominating, especially in the NCOOH-containing films where T2 remains only in the form of ridges (partially) outlining the T1 blobs. By AFM, dots are observed all over the NOH-containing films, again with greater height variation in the T2 regions between the blobs (see Figure SI-3, Supporting Information). For NCOOH-containing films, for which 1.5 mm/min is the morphological transition rate, both the T1 regions and the T2 ridges are characterized by a mixture of dots and short stripes (to varying proportions in different places), as shown by the AFM images in Figures 8 and SI-3, Supporting Information. The stripes (typically in small groups) are generally higher than the dots by about 5 nm, giving rise to irregular lateral undulation in T1 on the order of 0.5 μm (Figure 8).

At a dip-coating rate of 2 mm/min, the NCOOH system, which now shows only long, continuous stripes by AFM (Figure SI-4, Supporting Information), has relatively uniform film thickness corresponding to essentially pure T1. This dip-coating rate is consistently found to be the optimum rate (in the range investigated and for the composition studied) for obtaining films of uniform thickness. Increasing the dip-coating rate to 3, 4, and 5 mm/min leads to dewetting of the T1 layer, where the light color in Figure 6 is featureless in AFM and has a thickness of ca. 5 nm. The gray-colored regions by AFM show a mixed morphology where relatively narrow bands characterized by stripes (T1) alternate with broader featureless regions (Figure SI-5, Supporting Information) whose thickness ranges from ca. 10 nm for 3 mm/min to ca. 5 nm for 5 mm/min. The featureless regions must correspond to T0, an adsorbed brush layer of polymer with P4VP/NCOOH functioning as the

dx.doi.org/10.1021/ma3007398 | *Macromolecules* 2012, 45, 5463−5476

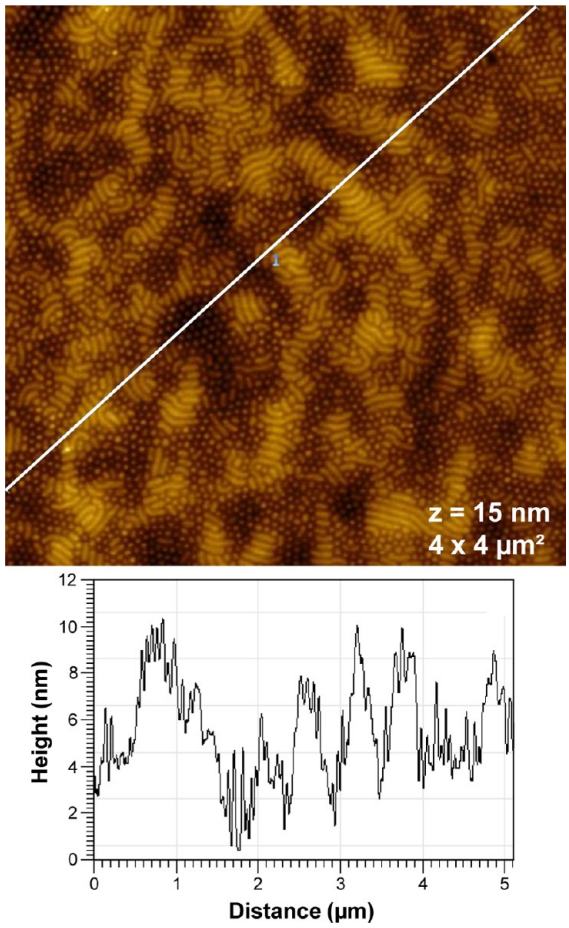

Figure 8. AFM height image of an equimolar PS−P4VP(41.5−17.5)/NCOOH film dip-coated at a rate of 1.5 mm/min. The height profile along the white line illustrates the significantly greater height of the stripes compared to the dots.

wetting layer on the polar substrate and PS lying on top due to its lower interfacial energy with air[23a,39] (see also the cross-sectional TEM results below). The fraction of the featureless regions coexisting with the stripe-patterned bands increases with dip-coating rate from 3 to 5 mm/min.

NOH-containing films dip-coated at 2 mm/min still show a small fraction of T2 regions in the OM images, while T1 predominates, and both regions continue to display the dot morphology in AFM (Figure SI-4, Supporting Information). These films reach their greatest uniformity in thickness for dip-coating rates of 3 to 5 mm/min. At 3 mm/min, the dot heights are much reduced so that this morphology is poorly visible in AFM (but rinsing with MeOH reveals pores; see Figure SI-5, Supporting Information), and not at all for 4 and 5 mm/min. The latter two films thus appear to be made up of a PS-covered P4VP/NOH brush layer, whereas the former appears to be on the verge of forming nodules (as if P4VP/NOH is in slight excess to what is needed for wetting). The thickness of the NOH-containing brush layer is 11 ± 2 nm, in comparison with 6 ± 2 nm for the NCOOH-containing brush layer, for films dip-coated at 4 and 5 mm/min. (It may be added that a very small fraction of thinner dewetted regions, ca. 2−3 nm in thickness, also appear here and there for PS−P4VP/NOH, fewer and thinner than for PS−P4VP/NCOOH at these dip-coating rates.) Step heights between terraces are more difficult to evaluate, due to the undulation within the T2 (and T3) layers, to the morphology change in the NCOOH system, and, probably, to nonequilibrium or kinetic aspects of the dewetting. However, we estimate the step heights to be about 20−25 nm.

The OM and AFM results combined show that BC ordering on a shorter length scale and terracing phenomena on a longer length scale both occur in the films studied. This takes place in a dip-coating regime that is dominated by capillary feeding of the depositing polymer solution as solvent evaporates; that is, capillary rise allows the solution to feed the upper part of the meniscus that forms on the substrate in contact with the solution as long as the motion of the drying line is slower than solvent evaporation.[22] As the dip-coating rate increases, capillary feeding decreases in importance, resulting in less and less deposited material, thus accounting for increasingly thin films. According to Meiners et al., the brush (wetting) layer is adsorbed onto the substrate in the solution before withdrawal of the substrate, with the additional material deposited during the withdrawal.[23d] This can explain why the minimum film thickness corresponds to this layer, and it implies that no additional material is adsorbed onto the substrate during withdrawal in this range. For conditions where additional layers (T1, T2, T3) are formed, they always show the same morphology in a given film, suggesting that it develops independently from the terracing phenomena.

The terracing observed can be related to dewetting phenomena, which are very complex and under intense study currently.[40] Perhaps the closest analogue to the present BC films, given the micellar nature of the dip-coating solutions, are colloidal suspensions, for which dewetting has received significant attention.[40,41] Particularly relevant is the work of Thiele and colleagues,[41] who showed that drop-cast films of colloidal suspensions typically undergo two steps of dewetting, the first in the form of a macroscopic front that is initially relatively fast and leaves behind a "postcursor" film. This is followed by mesoscopic dewetting of the "postcursor" film, which can result in various types of dewetting patterns involving evaporative and/or convective diffusion. Among the different patterns observed are polygonal structures of the type shown in Figure 6 for the slower dip-coating rates. These were successfully modeled by a kinetic Monte Carlo approach evolving from a nucleation and growth process of dewetting where the particles play a passive role (i.e., do not influence the dewetting patterns).[41a] Although the model considers only hard particles in a single layer, it seems reasonable that it applies qualitatively to the softer micelles of our solutions and for more than one layer. Thus, the micelles in the most slowly dip-coated films are effectively unperturbed relative to their solution state (i.e., dot morphologies only are obtained for both NOH- and NCOOH-containing films; see also the cross-sectional TEM results in the following section), and seem to behave passively with respect to the dewetting (the stripe morphology appears to be another matter, and possible reasons for its formation are discussed below). It is also reasonable to hypothesize, in this context, that the dewetting that leads to the patterns observed in OM, which are isotropic (i.e., show no orientation with respect to the substrate/solution interface), occurs more slowly than the withdrawal rate and thus takes place in a (presumably solvent-loaded) film no longer in contact with the solution, which can therefore be viewed as analogous to the "postcursor" film of ref 41.

In addition, it is noteworthy that the highest regions in the dewetted/terraced films are in the form of rims around the blobs, and close inspection of the three-level (T1, T2, T3)

dx.doi.org/10.1021/ma3007398 | *Macromolecules* 2012, 45, 5463−5476

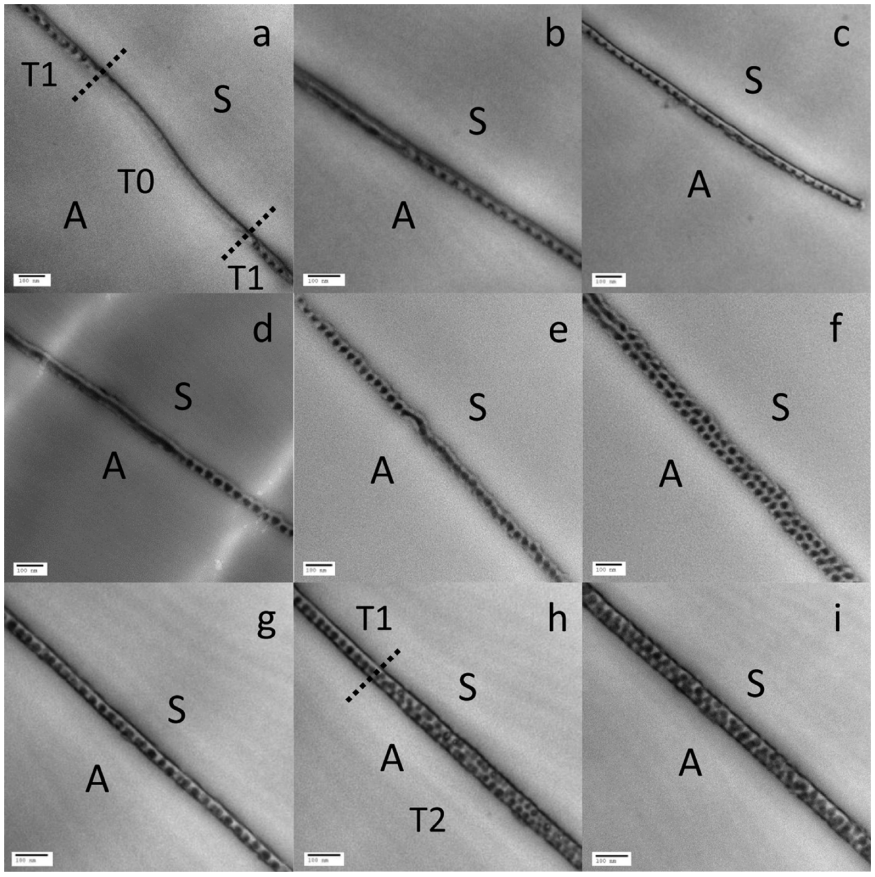

Figure 9. TEM micrographs of cross-sectional slices of I_2-stained 41.5−17.5 PS−P4VP/NCOOH thin films dip-coated at 2 (a, b, c), 1.5 (d, e, f) and 1 (g, h, i) mm/min, where the P4VP/NCOOH phase appears dark. The substrate (S) and air (A) sides of the slices are assigned based on the appearance of the wetting layer (see text). Scale bars: 100 nm.

images indicates that a rim also surrounds the T1 level (see Figures 7 and SI-2, Supporting Information). This is reminiscent of the "coffee ring" effect,[42] and has been modeled in ref 41a using mesoscale thin film hydrodynamics in relation to the self-pinning and depinning of increasingly concentrated contact (dewetting front) lines. The self-pinning occurs as the capillary rim carrying the dewetted liquid becomes sufficiently concentrated to approach random close packing, where the viscosity diverges.[41a] In this context, the terracing/dewetting of the material deposited during substrate retraction from solution onto the brush layer in the films shown in Figure 6 can be visualized as follows. Upon hole nucleation, a dewetting front in the form of a capillary rim[41a] moves outward carrying dewetted liquid that has not yet evaporated. The concentration of particles increases as the dewetting front moves to the outside leading to thicker film. Eventually, self-pinning of the dewetting liquid can occur to create a secondary layer. Expansion stops when the rim encounters another rim or when the film becomes too viscous. From this point of view, T0, T1, T2 (and eventually higher levels) might be viewed as resulting from self-pinning effects that occur during dewetting. The relative area percentage of the different levels is related to the amount of material adsorbed onto the substrate, which, in turn, depends on the withdrawal rate.

Cross-Sectional TEM. To access the out-of-plane structure of the thin films, particularly of PS−P4VP/NCOOH for dip-coating rates around the morphology transition, epoxy-embedded films were microtomed across their thickness (giving slices of about 70−80 nm thick) and stained with I_2 for TEM analysis. Representative TEM micrographs obtained at dip-coating rates of 2.0, 1.5, and 1.0 mm/min are shown in Figure 9. They capture segments of different film thicknesses resulting from the terracing phenomena, particularly corresponding to T0, T1, and T2.

A common feature in all of the images is a thin continuous dark line on the substrate side of the film (paler but still visible for the 1.5 mm/min film), which can be identified with stained P4VP (presumably containing NCOOH) that wets the substrate. In many cases, a thin unstained layer, which must be PS, separates the P4VP/NCOOH wetting layer from stained (i.e., P4VP-containing) objects lying above it. When not visible, it may be due to ultramicrotoming slightly off the perpendicular, which can give the illusion that some nonwetting stained objects are touching the wetting layer, or there may actually be interconnections with the wetting layer.

In examining the particularities of the images for different dip-coating rates, we will begin with the thinnest film, notably the one obtained at 2 mm/min, for which the images will be referred to as slices a, b, and c. In the central part of slice a, the only stained region is the wetting layer; thus this section must correspond to the T0 brush monolayer, visualized also by van Zoelen et al.[13a] for a PDP-containing PS−P4VP film. Here, the P4VP/NCOOH wetting layer is simply covered by the (unstained) PS layer, thus forming a lamella parallel to the substrate. The two end parts of slice a show, above the monolayer, a single row of isolated stained objects (P4VP/NCOOH) separated from one another by PS, indicating that these parts correspond to T1 segments. T1 segments are also

dx.doi.org/10.1021/ma3007398 | *Macromolecules* 2012, 45, 5463−5476

observed along the entire length of slices b and c, with a single row of isolated objects observed over more than half the length in each case. Since AFM indicates a stripe morphology for these films, the isolated objects must be sliced pieces of P4VP/NCOOH stripes lying across the slice. Part of a stripe lying parallel to the slice is apparent in slice b (top left end) and short sections of stripes lying at an angle can be perceived in the center of slice c. These stripes can be identified as cylinders lying parallel to the film plane. In some cases, especially in slices b (bottom right half) and c, the cylinders appear to be depressions and seem to be connected by a thin P4VP layer at the film surface. This might be related to exposure of the film surface to the HF water used to float it, which has a similar effect as MeOH exposure; i.e. washing up of P4VP to the film surface (possibly accompanied by loss of NCOOH) leaving P4VP-lined depressions or grooves.[10a,43,44]

Slices d, e and f correspond to cross-sectional slices of a film dip-coated at 1.5 mm/min, for which AFM shows coexisting dots and stripes. Slices d and e are composed of a T1 segment only and slice f of a T2 segment only. An in-plane cylinder section lying parallel to the slice runs along more than half of slice d. The quasi-circular objects in the other section of slice d (observed in slice e as well) could be spheres or sliced pieces of in-plane cylinders lying across the film slice. The central part of slice e appears to show a segment of an in-plane cylinder parallel to the slice, with a part that seems to be superposed by dots. This could be interpreted as a line of spheres in front of or behind a cylinder (relative to the slice), given that the microtomed slices are about twice as thick as the dot diameters or stripe thicknesses. But they may also be indicative of an intermediate state between spheres and a cylinder, where one form is transforming into the other via an undulated cylinder (as described, for example, in refs 8e and 45). Slice f of a T2 terrace shows two rows of quasi-circular objects lying displaced one relative to the other (in close-packed fashion). It is tempting to identify these objects with spheres, in which case the microtoming happened to take place almost perfectly along a lattice line; however, a series of horizontal cylinders (relative to the film plane) that lie across the slice cannot be ruled out. The bottom right part of slice f shows what appears to be a T2 cylinder segment lying horizontal to the film plane. For this film, there is no evidence of washing out of P4VP by HF water (i.e., there are no visible depressions on the film surface), possibly because the film was floated without its surface being exposed to the water (as should happen ideally, but is not necessarily the case in practice) or perhaps its surface is better protected by a thicker layer of PS, although there is a faint line of a stained overlayer indicative of a slight amount of P4VP on the film surface. (The much more weakly stained wetting and overlayers in this sample compared to the those dip-coated at 1 and 2 mm/min might be due to it having been exposed to I_2 vapor in a separate experiment from the other two albeit for the same length of time.)

Regarding the film dip-coated at 1 mm/min, for which only the dot morphology is observed by AFM, images of a T1 segment (slice g), a T2 segment (slice i), and segments of both terraces together (slice h), all from different places of the same microtomed slice, were captured. The single row of isolated quasi-circular objects above the wetting layer in slice g and the upper left part of slice h must be identified as spheres (i.e., cannot be in-plane cylinders perpendicular to the cross-section), given the AFM observations. The T2 segments are basically composed of two layers of quasi-circular objects, displaced one from the other as in slice f, but appearing less well-defined, less ordered and less isolated than in slice f. This might be caused, at least in part, to the microtoming having taken place at an angle to a lattice line of the spheres, therefore including parts of spheres from one or both neighboring lines within the slice thickness (i.e., perpendicular to the plane of the image). This can result in a form of doubling or even tripling of dots giving the illusion of closely spaced dots (as near the center of slice h) as well as some interconnectedness (as in slide i). It is thus not possible to ascertain with certainty from these images that the T2 segments here are composed of isolated spheres with no interconnections within the film. On the other hand, there is no evidence of vertically interconnected spheres or vertical cylinder morphology (relative to the film plane) in any of the images. At most, possibly budding interconnections (if not an illusion) occur at an angle to the vertical that corresponds to two vertically displaced rows of spheres, and forming a kind of zigzag pattern (slice i). Likewise, none of the images of the 1 mm/min film show any evidence of horizontal cylinders in the lower layer of T2 terraces (which, in principle, might have been a possibility, since AFM shows only the surface). Finally, it is noteworthy that the transition between the T1 and T2 segments in slice h appears to occur progressively over a range of several dots (approximately 100−150 nm), and not as an abrupt thickness change.

Lateral Periodicities. Table 3 includes a comparison of the lateral periodicities (spacings) measured from AFM images of films that were dip-coated from both NOH- and NCOOH-containing solutions (equimolar SM:VP) at various rates. It can be observed, first of all, that the largest periodicities measured for the 41.5−17.5 and 78.9−30.3 systems are very similar to the hydrodynamic diameters (i.e., twice R_h) obtained from the light-scattering data for these systems. A similar observation correlating micellar size in solution and in dried dip-coated films was made by Meiners et al. for PS−P2VP and taken to indicate that entire micelles are adsorbed onto the surface during the film-forming process.[23d]

Several trends in the periodicities can be pointed out. For the dot morphology, the periodicities tend to increase with dip-coating rate, or, in other words, with decrease in average film thickness (the small differences between the fewer points available for the stripe morphology do not allow detection of a clear trend). This correlates well with the (much weaker) tendency observed by Knoll et al. within a given terrace for in-plane cylinder-forming films of triblock copolymers (spin-coated and annealed in $CHCl_3$).[46] In fact, they found that the periodicity displays a sawtooth pattern as a function of film thickness, where the decreasing periodicity value with increase in thickness in a given terrace jumps to the higher periodicity value whenever an additional terrace is formed. Lambooy et al. also observed a sawtooth pattern in the periodicity as a function of film thickness (centered around the equilibrium periodicity) for a confined multilayer lamellar diblock copolymer.[47] Here, the periodicity in a film of n layer increases with film thickness, and then jumps to the lowest periodicity at the transition to n + 1 layers.

In our case, for two different terraces in a dot-patterned film, the periodicity of the lower terrace is greater than that in the higher terrace. Furthermore, around a dot-stripe morphology transition, the stripe periodicity is lower than the dot periodicity. This can be correlated with the observation made above that, for coexisting stripes and dots (Figure 8), the stripes are always higher than the dots. Finally, it is observed that, for a

dx.doi.org/10.1021/ma3007398 | Macromolecules 2012, 45, 5463−5476

given copolymer dip-coated under the same conditions, the periodicity in the NOH-containing films is always significantly lower than that in the NCOOH-containing films, both for stripes vs dots and for dots vs dots. It is difficult to rationalize all of these trends at this time, since the forces involved in the film-forming process (capillary feeding, solvent evaporation, dewetting, etc.) are complex. However, it is noteworthy that, in the 78.9−30.3 system, the periodicity of the dot morphology of the NOH-containing films at the highest dip-coating rate used is close to that of the NCOOH-containing system just before the transition to the stripe morphology (the trend seems similar in the 41.5−17.5 system albeit less clear due to the fewer data points available). Since greater distances may be related to increased chain extension (assuming that the nodules are indeed adsorbed micelles from solution, and therefore unchanged in average diameter from that in solution except for some degree of shrinkage following solvent evaporation), this suggests that the transition from dots to stripes occurs when the maximum chain extension relative to other equilibrating forces is reached. This can also explain, at least in part, the sudden decrease of the spacing, to relieve the stretching forces, in transitioning from dots to stripes.

Dot vs Stripe Morphology. It is noteworthy that the stripe morphology is observed only in the thinner, more rapidly dip-coated films, never in the thicker, more slowly dip-coated films (for the compositional and experimental conditions investigated). It is also more favored in films with NCOOH than in films with NOH, as well as when using higher solution concentrations or higher SM:VP ratios. The dot morphology (which TEM indicates are essentially spheres and not vertical cylinders) most likely results from the deposition of the spherical micelles found in solution and that are frozen in by relatively rapid solvent evaporation, whereas the stripe morphology (which TEM indicates are in-plane cylinders and not side-on lamellae) involves a perturbation of the micelles leading to morphological rearrangement. Given the complexity of the dip-coating process and subsequent dewetting, we can only speculate about the reasons for the transition to the stripe morphology, touching briefly on several considerations.

One consideration is the respective swelling of the P4VP and PS phases by the SM and solvent (THF) in the concentrated film deposited on the substrate, and how this might evolve as solvent continues to evaporate. In the drying film, THF swells the PS phase much more than the P4VP phase, which is the reason for the film topography of the lower-lying PS matrix compared to P4VP/SM protrusions, as explained earlier. The SM is expected to be concentrated in the P4VP phase due to H-bond attraction. However, in the dip-coating solution itself, there is no significant swelling of the P4VP micelle cores by the SM, as indicated by the LS results, implying that the SM is mainly freely dissolved in the THF, and only H-bonds with P4VP as THF evaporates from the deposited film. In the process, some of the SM in the film may be located in the PS phase, possibly to differing extents for NOH and NCOOH. Indeed, DSC measurements of films of PS that were solution-blended with the SMs indicate some miscibility of both SMs in PS, but more for NOH than for NCOOH.[48] Furthermore, because NCOOH H-bonds more strongly than NOH to P4VP, it may experience greater selectivity than NOH for the P4VP phase. Both effects can have the result that, for the same total amount of SM in the two types of films, the P4VP core is swelled more by NCOOH than by NOH. With the additional finding that the SM:VP ratio in the film is less than that in solution at very slow dip-coating rates, that it increases with dip-coating rate, and that it is the same for both SMs when dip-coated in identical conditions,[30] it is reasonable to postulate the following. First, the increasing SM:VP ratio shifts the relative phase fractions such that the spherical morphology in the (probably solvent-laden) deposited film shifts to cylindrical morphology, thus accounting for its appearance in the thinner films where the SM:VP ratio is highest. Second, if the sequestering of the SM in the P4VP phase is greater for NCOOH than for NOH, then it is reasonable that this phase transition is more favored in NCOOH-containing films (for the same total amount of SM), as observed. This is further supported by the fact that a higher SM:VP solution ratio favors the stripe morphology.

A different aspect to consider relates to a previous observation that PS−P4VP micellar solutions are subject to deaggregation by shear (such as in standard viscometry tubes), although with quick recovery upon cessation of shear.[34] This indicates that the micelles can be perturbed relatively easily. In the thinnest films, shear forces between the flowing solution and solid substrate may exert an effect on the morphology. Conceivably, the stronger NCOOH−VP H-bond compared to the NOH−VP H-bond makes NCOOH-containing films more sensitive to shear forces than NOH-containing films. The possible contribution of shear effects can also rationalize the observations that higher SM:VP ratio and higher solution concentration favor stripes, in that greater shear effects can be attributed to increased H-bonding and to increased solution viscosity, respectively. Furthermore, shear forces can be a source of increased chain stretching between the micelles, which, when exceeding what can be tolerated, may provoke the morphology change to stripes.

A third aspect to consider is the size of the micelles in solution compared to the solvent-laden film thickness. For example, if the depositing film (meniscus) becomes too thin compared to the micelle size, the latter may tend to accumulate at the solution/substrate interface, which may provoke fusion into cylinders. This could constitute another possible reason that NCOOH and higher SM:VP ratios, if they lead to larger P4VP/NCOOH micelle cores in concentrated solution, favor stripes. An effect of this type was observed by Ghosh et al. for hard particles, which deposit in the form of bands parallel to the substrate/solution interface.[49] In our case, the much softer cylinders, possibly coupled with capillary feeding causing convection, may result in meandering, i.e. nondirectional, stripes.

Clearly, more investigations must be forthcoming to understand more fully the phenomena, particularly morphology evolution, in dip-coated supramolecular block copolymer films. Besides the effects of film thickness[1] (determined here by dip-coating rate), of SM content in the films (also determined by dip-coating rate[30]) and SM distribution between block domains, and perhaps of shear forces or pinning effects, as discussed above, other effects such as the type of solvent, solvent evaporation rate (which also varies with film thickness[50]) and interrelationships between different effects must be taken into account.

■ CONCLUSIONS

The results described above show that the use of NCOOH versus NOH, which differ only by the functional hydrogen-bonding substituent, to exert a supramolecular control over dip-coated thin film morphology can indeed provide drastically

different morphologies. With NCOOH, stripe morphologies were obtained in a relatively large range of experimental and compositional conditions, whereas with NOH, the dot morphology was obtained in almost all of the same conditions, including for identical film thicknesses. In searching for the underlying cause(s) of the differences observed, a number of findings were made. Compared to the dot morphology, the stripe morphology is favored not only by NCOOH, but also by higher solution concentrations, dip-coating rates, and SM:VP ratios. Light scattering indicates that the solutions are composed of spherical micelles, which are of similar size whether containing PS−P4VP alone or mixed with either SM (equimolar SM:VP), and infrared analysis indicates that the films contain the same total amount of SM for identical dip-coating conditions, thus eliminating that these characteristics can account for the different morphologies. Cross-sectional TEM showed that the dot morphology is essentially composed of micelles, indicating that the solution micelles are deposited on the substrate without morphological rearrangement, whereas the stripes are in-plane cylinders.

Importantly, it was found that the average film thickness (or amount of material deposited) decreases with increase in dip-coating rate to a minimum thickness that corresponds essentially to where a brush layer of the block copolymer is adsorbed to the substrate. This puts the dip-coating conditions, involving very slow dip-coating rates, in the recently described "capillarity regime", seldom explored in general and never in conjunction with an evolution in block copolymer morphology. The real film thicknesses are variable due to dewetting phenomena resulting in terraces. Possible reasons for the stripe morphology are discussed in terms of SM content and degree of P4VP selectivity in the films and in terms of possibly greater shear forces or accumulation effects in very thin NCOOH- compared to NOH-containing films, all of which can be influenced by the hydrogen bond strength with P4VP, which is greater for NCOOH than for NOH.

■ ASSOCIATED CONTENT

Supporting Information

Infrared spectra of systems involving other functional small molecules and additional AFM images of the dewetting/terracing phenomena. This material is available free of charge via the Internet at http://pubs.acs.org.

■ AUTHOR INFORMATION

Corresponding Author

*E-mail: (C.G.B.) geraldine.bazuin@umontreal.ca; (R.E.P.) re.prudhomme@umontreal.ca.

Notes

The authors declare no competing financial interest.

■ ACKNOWLEDGMENTS

The financial support of NSERC Canada and FQRNT Québec is gratefully acknowledged. Dr. Alexis Laforgue is thanked for initiating DG to the research and for the in-plane TEM results. We also thank Prof. Antonio Nanci, Sylvia Francis Zalzal, and Cynthia Török of the Faculté de médecine dentaire of Université de Montréal for access to the instrumentation for, and assistance with, obtaining the cross-sectional TEM results.

■ REFERENCES

(1) Fasolka, M. J.; Mayes, A. M. *Annu. Rev. Mater. Res.* **2001**, *31*, 323−355.
(2) (a) Hamley, I. W. *Angew. Chem., Int. Ed.* **2003**, *42*, 1692−1712. (b) Hamley, I. W. *Prog. Polym. Sci.* **2009**, *34*, 1161−1210.
(3) Li, M.; Coenjarts, C. A.; Ober, C. K. *Adv. Polym. Sci.* **2005**, *190*, 183−226.
(4) Darling, S. B. *Prog. Polym. Sci.* **2007**, *32*, 1152−1204.
(5) Olson, D. A.; Chen, L.; Hillmyer, M. A. *Chem. Mater.* **2008**, *20*, 869−890.
(6) van Zoelen, W.; ten Brinke, G. *Soft Matter* **2009**, *5*, 1568−1582.
(7) Marencic, A. P.; Register, R. A. *Annu. Rev. Chem. Biomol. Eng.* **2010**, *1*, 277−297.
(8) (a) Sidorenko, A.; Tokarev, I.; Minko, S.; Stamm, M. *J. Am. Chem. Soc.* **2003**, *125*, 12211−12216. (b) Tokarev, I.; Krenek, R.; Burkov, Y.; Schmeisser, D.; Sidorenko, A.; Minko, S.; Stamm, M. *Macromolecules* **2005**, *38*, 507−516. (c) Luchnikov, V.; Kondyurin, A.; Formanek, P.; Lichte, H.; Stamm, M. *Nano Lett.* **2007**, *7*, 3628−3632. (d) Böhme, M.; Kuila, B.; Schlörb, H.; Nandan, B.; Stamm, M. *Phys. Status Solidi B* **2010**, *247*, 2458−2469. (e) Nandan, B.; Vyas, M. K.; Böhme, M.; Stamm, M. *Macromolecules* **2010**, *43*, 2463−2473. (f) Kuila, B.; Stamm, M. *J. Mater. Chem.* **2011**, *21*, 14127−14134. (g) Seifarth, O.; Krenek, R.; Tokarev, I.; Burkov, Y.; Sidorenko, A.; Minko, S.; Stamm, M.; Schmeisser, D. *Thin Solid Films* **2007**, *515*, 6552−6556.
(9) (a) Liang, C.; Hong, K.; Guiochon, G. A.; Mays, J. W.; Dai, S. *Angew. Chem., Int. Ed.* **2004**, *43*, 5785−5789. (b) Tung, S.-H.; Kalarickal, N. C.; Mays, J. W.; Xu, T. *Macromolecules* **2008**, *41*, 6453−6462. (c) Tung, S.-H.; Xu, T. *Macromolecules* **2009**, *42*, 5761−5765. (d) Lee, C.-H.; Tung, S.-H. *Soft Matter* **2011**, *7*, 5660−5668. (e) Huang, W.-H.; Chen, P.-Y.; Tung, S.-H. *Macromolecules* **2012**, *45*, 1562−1569.
(10) (a) Laforgue, A.; Bazuin, C. G.; Prud'homme, R. E. *Macromolecules* **2006**, *39*, 6473−6482. (b) Laforgue, A.; Gaspard, D.; Bazuin, C. G.; Prud'homme, R. E. *Am. Chem. Soc. Polym. Prepr.* **2007**, *48* (1), 670−671.
(11) Zhang, P.; Gao, J.; Li, B.; Han, Y. *Macromol. Rapid Commun.* **2006**, *27*, 295−301.
(12) Rodriguez, A. T.; Li, X.; Wang, J.; Steen, W. A.; Fan, H. *Adv. Funct. Mater.* **2007**, *17*, 2710−2716.
(13) (a) van Zoelen, W.; Asumaa, T.; Ruokolainen, J.; Ikkala, O.; ten Brinke, G. *Macromolecules* **2008**, *41*, 3199−3208. (b) van Zoelen, W.; Polushkin, E.; ten Brinke, G. *Macromolecules* **2008**, *41*, 8807−8814. (c) van Zoelen, W.; Bondzic, S.; Landaluce, T. F.; Brondijk, J.; Loos, K.; Schouten, A.-J.; Rudolf, P.; ten Brinke, G. *Polymer* **2009**, *50*, 3617−3625.
(14) Son, J. G.; Bulliard, X.; Kang, H.; Nealey, P. F.; Char, K. *Adv. Mater.* **2008**, *20*, 3643−3648.
(15) Hagaman, D.; Enright, T. P.; Sidorenko, A. *Macromolecules* **2012**, *45*, 275−282.
(16) (a) Mayes, A. M.; Russell, T. P.; Satija, S. K.; Majkrzak, C. F. *Macromolecules* **1992**, *25*, 6523−6531. (b) Jeong, U.; Ryu, D. Y.; Kim, J. K.; Kim, D. H.; Wu, X.; Russell, T. P. *Macromolecules* **2003**, *36*, 10126−10129. (c) Jeong, U.; Ryu, D. Y.; Kim, J. K.; Kim, D. H.; Russell, T. P.; Hawker, C. J. *Adv. Mater.* **2003**, *15*, 1247−1250. (d) Kim, S. H.; Misner, M. J.; Russell, T. P. *Adv. Mater.* **2004**, *16*, 2119−2123.
(17) Gao, J.; Zhang, P.; Fu, J.; Li, B.; Han, Y.; Yu, X.; Pan, C. *Polymer* **2007**, *48*, 2425−2433.
(18) Guo, R.; Huang, H.; Chen, Y.; Gong, Y.; Du, B.; He, T. *Macromolecules* **2008**, *41*, 890−900.
(19) Stuen, K. O.; Thomas, C. S.; Liu, G.; Ferrier, N.; Nealey, P. F. *Macromolecules* **2009**, *42*, 5139−5145.
(20) Lee, W.; Zhang, X.; Briber, R. M. *Polymer* **2010**, *51*, 2376−2382.
(21) (a) Ruokolainen, J.; Mäkinen, R.; Torkkeli, M.; Mäkelä, T.; Serimaa, R.; ten Brinke, G.; Ikkala, O. *Science* **1998**, *280*, 557−560. (b) Ruokolainen, J.; Saariaho, M.; Ikkala, O.; ten Brinke, G.; Thomas, E. L.; Torkkeli, M.; Serimaa, R. *Macromolecules* **1999**, *32*, 1152−1158. (c) Ruokolainen, J.; ten Brinke, G.; Ikkala, O. *Adv. Mater.* **1999**, *11*,

777−780. (d) Bondzic, S.; de Wit, J.; Polushkin, E.; Schouten, A. J.; ten Brinke, G.; Ruokolainen, J.; Ikkala, O.; Dolbnya, I.; Bras, W. *Macromolecules* **2004**, *37*, 9517−9524.
(22) (a) Faustini, M.; Louis, B.; Albouy, P. A.; Kuemmel, M.; Grosso, D. *J. Phys. Chem. C* **2010**, *114*, 7637−7645. (b) Grosso, D. *J. Mater. Chem.* **2011**, *21*, 17033−17038.
(23) (a) Meiners, J. C.; Ritzi, A.; Rafailovich, M. H.; Sokolov, J.; Mlynek, J.; Krausch, G. *Appl. Phys. A: Mater. Sci. Process.* **1995**, *61*, 519−524. (b) Li, Z.; Zhao, W.; Liu, Y.; Rafailovich, M. H.; Sokolov, J.; Khougaz, K.; Eisenberg, A.; Lennox, R. B.; Krausch, G. *J. Am. Chem. Soc.* **1996**, *118*, 10892−10893. (c) Meiners, J. C.; Elbs, H.; Ritzi, A.; Mlynek, J.; Krausch, G. *J. Appl. Phys.* **1996**, *80*, 2224−2227. (d) Meiners, J. C.; Quintel-Ritzi, A.; Mlynek, J.; Elbs, H.; Krausch, G. *Macromolecules* **1997**, *30*, 4945−4951.
(24) The cleaning procedure used, the rate of substrate immersion and the length of time immersed were found not to influence the thin film morphologies obtained, according to our previous study involving another hydrogen-bonding small molecule.[10a]
(25) Lee, J. Y.; Painter, P. C.; Coleman, M. M. *Macromolecules* **1988**, *21*, 954−960.
(26) Cesteros, L. C.; Isasi, J. R.; Katime, I. *Macromolecules* **1993**, *26*, 7256−7262.
(27) Sallenave, X.; Bazuin, C. G. *Macromolecules* **2007**, *40*, 5326−5336.
(28) Brandys, F. A.; Bazuin, C. G. *Chem. Mater.* **1996**, *8*, 83−92.
(29) Kato, T.; Kihara, H.; Uryu, T.; Fujishima, A.; Fréchet, J. M. J. *Macromolecules* **1992**, *25*, 6836−6841.
(30) Roland, S.; Pellerin, C.; Prud'homme, R. E.; Bazuin, C. G. *Am. Chem. Soc., Polym. Prepr.* **2011**, *52* (1), 101−102. Roland, S.; Pellerin, C.; Bazuin, C. G.; Prud'homme, R. E. *Macromolecules* **2012**, submitted for publication.
(31) Elbs, H.; Fukunaga, K.; Stadler, R.; Sauer, G.; Magerle, R.; Krausch, G. *Macromolecules* **1999**, *32*, 1204−1211.
(32) Park, S.; Wang, J.-Y.; Kim, B.; Xu, J.; Russell, T. P. *ACS Nano* **2008**, *2*, 766−772.
(33) Kuila, B. K.; Gowd, E. B.; Stamm, M. *Macromolecules* **2010**, *43*, 7713−7721.
(34) Antonietti, M.; Heinz, S.; Schmidt, M.; Rosenauer, C. *Macromolecules* **1994**, *27*, 3276−3281.
(35) Antonietti, M.; Bremser, W.; Schmidt, M. *Macromolecules* **1990**, *23*, 3796−3805.
(36) (a) Huang, L. C.; Richman, E. K.; Kirsch, B. L.; Tolbert, S. H. *Microporous Mesoporous Mater.* **2006**, *96*, 341−349. (b) Yimsiri, P.; Mackley, M. R. *Chem. Eng. Sci.* **2006**, *61*, 3496−3505.
(37) Some values from the early studies may not be averages, leading to greater scatter in the data; however, the trends in Figure 5 remain clear and are consistent with the equation in ref 22.
(38) Landau, L.; Levich, B. *Acta Phys. Chim. U.R.S.S.* **1942**, *17*, 42−54.
(39) Karim, A.; Singh, N.; Sikka, M.; Bates, F. S.; Dozier, W. D.; Felcher, G. P. *J. Chem. Phys.* **1994**, *100*, 1620−1629.
(40) Stannard, A. *J. Phys: Condens. Matter* **2011**, *23*, 083001.
(41) (a) Thiele, U.; Vancea, I.; Archer, A. J.; Robbins, M. J.; Frastia, L.; Stannard, A.; Pauliac-Vaujour, E.; Martin, C. P.; Blunt, M. O.; Moriarty, P. J. *J. Phys.: Condens. Matter* **2009**, *21*, 264016. (b) Pauliac-Vaujour, E.; Stannard, A.; Martin, C. P.; Blunt, M. O.; Notingher, I.; Moriarty, P. J.; Vancea, I.; Thiele, U. *Phys. Rev. Lett.* **2008**, *100*, 176102.
(42) Deegan, R. D.; Bakajin, O.; Dupont, T. F.; Huber, G.; Nagel, S. R.; Witten, T. A. *Nature* **1997**, *389*, 827−829.
(43) (a) Qiao, Y.; Wang, D.; Buriak, J. M. *Nano Lett.* **2007**, *7*, 464−469. (b) Chai, J.; Wang, D.; Fan, X.; Buriak, J. M. *Nature Nano* **2007**, *2*, 500−506.
(44) Lin, Y.; Böker, A.; He, J.; Sill, K.; Xiang, H.; Abetz, C.; Li, X.; Wang, J.; Emrick, T.; Long, S.; Wang, Q.; Balazs, A.; Russell, T. P. *Nature* **2005**, *434*, 55−59 Supporting Information.
(45) Kimishima, K.; Koga, T.; Hashimoto, T. *Macromolecules* **2000**, *33*, 968−977.
(46) Knoll, A.; Tsarkova, L.; Krausch, G. *Nano Lett.* **2007**, *7*, 843−846.
(47) Lambooy, P.; Russell, T. P.; Kellogg, G. J.; Mayes, A. M.; Gallagher, P. D.; Satija, S. K. *Phys. Rev. Lett.* **1994**, *72*, 2899−2902.
(48) For films of polystyrene (110k) solution-blended in THF with 9 wt % SM, DSC (9 °C/min, using the modulation mode) showed a T_g of 71 and 80 °C for the NOH- and NCOOH-containing blends, respectively, compared to 90 °C for pure PS prepared in the same way.
(49) Ghosh, M.; Fan, F.; Stebe, K. J. *Langmuir* **2007**, *23*, 2180−2183.
(50) Phillip, W. A.; Hillmyer, M. A.; Cussler, E. L. *Macromolecules* **2010**, *43*, 7763.